

Decoupled Strain Response of Ferroic Properties in Multiferroic VOCl_2 Monolayer

Akshay Mahajan^{1,*} and Somnath Bhowmick^{1,†}

¹*Department of Materials Science and Engineering,
Indian Institute of Technology, Kanpur, Kanpur 208016, India*

(Dated: February 17, 2022)

Two-dimensional (2D) magnetoelectric multiferroics are promising multifunctional materials for miniaturized logic and memory devices. Herein, we explore the effectiveness of strain-engineering for tuning the properties of a recently predicted 2D antiferromagnetic-ferroelectric, VOCl_2 monolayer. Interestingly, we find that magnetic-ordering and electric polarization can be tuned independently using uniaxial tensile strain along different in-plane lattice vectors. A 4% tensile strain along lattice vector b induces a transition from an antiferromagnetic (AFM) ground state with an out-of-plane magnetization to a ferromagnetic (FM) ground state with in-plane magnetization. On the other hand, tensile strain along lattice vector a enhances spontaneous electric polarization, without affecting the magnetic ordering. The monolayers remain dynamically stable under tensile strain, which further helps to raise the Curie temperature of ferromagnetism, as well as ferroelectricity. Such a strain-tunable multiferroic material holds great promises for future generation nanoelectronic devices.

I. INTRODUCTION

Magnetoelectric multiferroics^{1–3} have fascinated materials scientists and engineers for the last two decades with their rich fundamental physics of combining electronic and magnetic properties and its applications for nanoelectronics. This unique characteristic of combining electric and magnetic ferroic properties makes them potential multifunctional materials for designing devices where a single device component can perform more than one task. This quality is especially desirable for the miniaturization of devices⁴. Among these multiferroics, particular significance is given to ferromagnetic-ferroelectric (FM-FE) materials, which can be used for new device architectures based on four logic states^{5,6}.

Realization of enhanced multiferroic properties, e.g., enlarged polarization in thin-films of three-dimensional (3D) multiferroics, have further stimulated multiferroic research for miniaturized non-volatile logic and memory devices^{7–10}. However, these thin films have limitations due to the requirement of a critical thickness for sustaining the ferroelectric (FE) state due to the effects of surface, depolarizing electrostatic field, and electron screening^{11–16}. Therefore, for the advancement of nanoelectronics, new low-dimensional multiferroics are required. Recently, using first-principles simulations, various two-dimensional (2D) magnetic^{17–21}, ferroelectric^{22–24}, and multiferroic materials have been discovered²⁵. Several approaches, including intercalation^{26,27}, doping²⁸, and defect engineering²⁹, have been used to design 2D FE ferromagnetism. Various other multiferroics have also been discovered^{30–34}; most of them belonging to the type-I² category, where ferroelectricity and magnetism have independent origins with high polarization values but relatively weak magnetoelectric coupling. The type-II² multiferroics, where the magnetic arrangements induce ferroelectricity and thus results in strong magnetoelectric coupling with smaller polarization values, are quite rare. To the best of our

knowledge, MXene $\text{Hf}_2\text{VC}_2\text{F}_2$ monolayer³⁵ is the only type-II multiferroic, among 2D materials.

Single-phase one-cation type-I multiferroic monolayers VOX_2 ($X = \text{Cl}, \text{Br}, \text{I}$) family^{36,37} is an interesting new addition to the ever increasing list of 2D multiferroics. These monolayers have been demonstrated to violate the d^0 rule in multiferroics.^{37,38} Generally, it has been observed that the partial occupancy of d-orbitals of transition metal cations, which is essential for the origin of magnetism, suppresses the occurrence of ferroelectricity. However, in VOX_2 monolayers, d^0 rule gets violated since the partially occupied d-orbital lies in a plane perpendicular to the ferroelectric polarization and such a configuration even helps to enhance the electric polarization in these monolayers.³⁷

Among VOX_2 family of 2D multiferroics, VOCl_2 monolayer has been predicted as an easily exfoliable 2D antiferromagnetic-ferroelectric (AFM-FE) having an in-plane spontaneous electric polarization and an out-of-plane magnetization.³⁶ In this work, using first-principle calculations, we demonstrate that the magnetic ordering in VOCl_2 can be tuned via strain-engineering, along with the enhancement of electric polarization. The transition from AFM-FE to FM-FE state takes place at around 4% in-plane biaxial tensile strain, which also leads to significant enhancement ($\sim 14\%$) of electric polarization. We further establish that, the uniaxial strain along the in-plane lattice vector b and a is separately responsible for the change in ground-state magnetic ordering and increase in the FE polarization, respectively. Increasing energy barrier for polarization switching, as well as an enhancement of magnetic exchange coupling parameter predicts both ferroelectric and ferromagnetic Curie temperature to increase with increasing tensile strain. The dependence of the ferroelectric switching energy barrier on the ground state magnetic ordering also suggests some kind of magnetoelectric coupling. A comparison of magnetocrystalline anisotropy energies also reveal a 90° rotation of magnetization direction, associated with the tran-

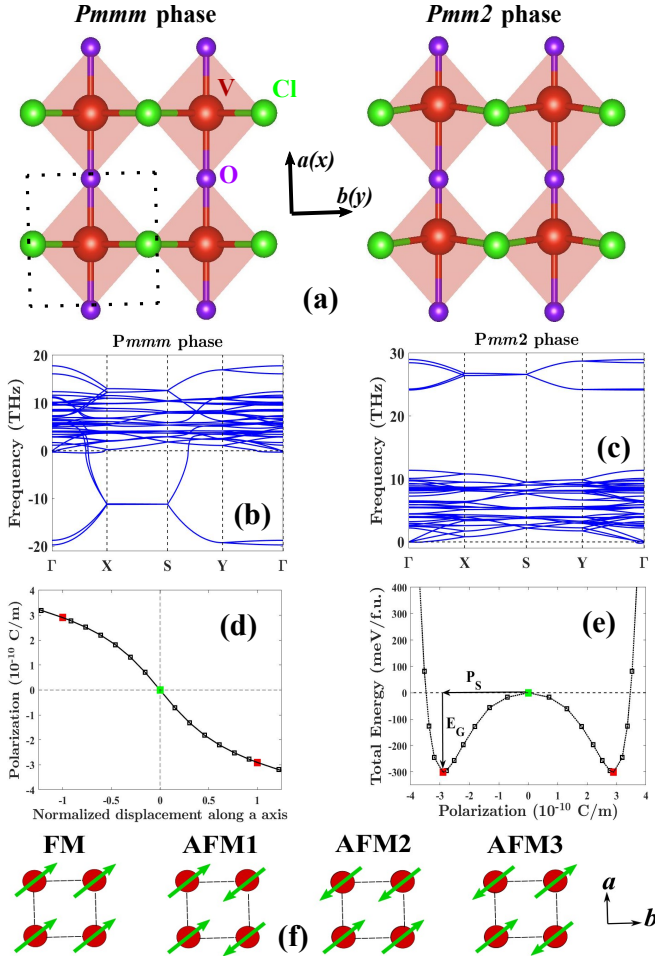


FIG. 1. (a) Top views of the high ($Pmmm$) and low-symmetry ($Pmm2$) VOCl_2 monolayers. Black dotted rectangle denotes the primitive cell (containing an octahedron). Phonon spectra of the (b) $Pmmm$ and (c) $Pmm2$ phases, respectively. (d) Calculated total polarization as a function of normalized displacement along the adiabatic path. (e) Double-well potential of VOCl_2 monolayer. Green and red squares in (d) and (e) represent PE ($Pmmm$) and FE ($Pmm2$) phases, respectively. (f) Schematic of four different magnetic configurations considered, showing only V atoms [compare with panel (a)].

sition from the state of AFM-FE (out of plane) to FM-FE (in plane).

Scope of tuning a 2D ferroelectric material (having in-plane electric polarization) via applying strain along the polar axis has recently been explored in several studies.^{39,40} However, to the best of our knowledge, this is the first report on strain engineering of a 2D multiferroic material, showing that different ferroic properties can be *independently* controlled via applying strain along different in-plane crystallographic directions, which makes VOCl_2 a very promising material for next generation nanoelectronic devices. The paper is organized as follows: In Section II, we present the computational details, followed by the results and discussions in Section III and the paper is concluded in Section IV.

II. COMPUTATIONAL DETAILS

All first-principles calculations are performed within the framework of density functional theory (DFT) using a plane-wave basis set, as implemented in the VASP suite of codes.^{41–43} Projector augmented wave (PAW)^{44,45} pseudopotentials are used in which exchange and correlation effects are treated within a generalized gradient approximation (GGA) scheme, developed by Perdew-Burke-Ernzerhof (PBE).⁴⁶ For all structural relaxation and electronic structure calculations, except the phonon spectra calculations, vdW-DF2^{47–50} non-local correlation functional is used to account for dispersion interactions. For DFT+U based calculations, effective U values are added according to the method proposed by Dudarev *et al.*⁵¹ 2D VOCl_2 monolayer is exfoliated from its 3D parent, which is retrieved from the Inorganic Crystal Structure Database (ICSD)⁵² with ICSD number 24380. All calculations are done for a $2 \times 2 \times 1$ supercell of VOCl_2 unit cell to consider different magnetic orderings. A vacuum layer of 20 Å is added along c -axis (z -direction) to avoid the spurious interaction between the monolayer and its periodic images. An energy cutoff of 520 eV is used for the plane-wave basis set with a k -mesh of $7 \times 7 \times 1$ for the Brillouin zone (BZ) integrations. For structural relaxation, a criterion of 0.001 eV/Å for the Hellman-Feynman forces is used, and optimization of atomic positions and lattice constants are done using a conjugate gradient (CG) algorithm. The phonon spectra are calculated using the linear response method, which utilizes density functional perturbation theory (DFPT), as implemented in Phonopy.⁵³ The electric polarization is calculated using the Berry phase method.^{54,55} The magnetocrystalline anisotropy energy (MAE) is calculated using the magnetic force theorem.^{56–58} Note that, the spin-orbit coupling (SOC) is taken into account only for the MAE calculations. The convergence of the MAE with respect to the k -point sampling has been tested by performing calculations for the unstrained AFM3 monolayer, using up to $14 \times 14 \times 1$ k -point mesh and we find that a $7 \times 7 \times 1$ mesh is sufficient for convergence of the MAE values (to about $\pm 1 \mu\text{eV/f.u.}$). Tensile strain along different lattice parameters is defined as $\varepsilon = (a - a_0)/a_0 = (b - b_0)/b_0$, where a , b are in-plane lattice parameters and a_0 , b_0 are the equilibrium lattice constants for the unstrained AFM3 VOCl_2 monolayer.

III. RESULTS AND DISCUSSIONS

The top view of the crystal structure of the VOCl_2 monolayer is illustrated in Figure 1(a). Among the two phases, namely the paraelectric (PE) $Pmmm$ and FE $Pmm2$, the V ion along the V-O chain (parallel to the polar axis or a -axis) is displaced in the latter. The V ion displacement lifts the inversion center present in the PE phase within the VO_2Cl_4 octahedra [Figure S1 of Supplemental Material⁵⁹], leading to a spontaneous po-

larization. The phonon spectra of PE and FE phases [Figure 1(b) and 1(c)] reveals the presence of soft optical modes in the former (arising because of the displacement of the V ion); suggesting spontaneous symmetry breaking below the Curie temperature, causing the transition from the high-symmetry PE phase to the low-symmetry FE phase.⁶⁰ Figure 1(d) shows the variation of total polarization of the VOCl_2 monolayer as a function of the V ion displacement along the polar axis (a -axis), which confirms the direct proportionality of the electric polarization to the amount of V ion's displacement from the inversion center. The polarization-displacement curve also displays how the sign of the polarization depends on the direction of V ion displacement along the polar axis. The characteristic marker of spontaneous electric polarization, the double-well potential, is also plotted in Figure 1(e). From the double-well potential, spontaneous electric polarization (P_S) value of 2.9×10^{-10} C/m and a potential barrier (E_G) of 301 meV per cation [or per formula unit (f.u.)] is determined, which are similar to the values predicted in earlier works.^{36,37}

We consider four different magnetic states, ferromagnetic (FM) and three different types of anti-ferromagnetic (AFM1, AFM2, AFM3) orders, schematically illustrated in Figure 1(f), where only V ions are shown for clarity [compare with 1(a)]. Study of AFM ordering requires a $2 \times 2 \times 1$ supercell. According to our first-principles calculations, among the four magnetic orders, the ground-state magnetic ordering is AFM3. Figure 2(a) shows the electronic band structure of the AFM3 VOCl_2 monolayer, along with orbital projected density of states (PDOS) plot illustrated in Figure 2(b). Evidently, VOCl_2 monolayer has an indirect band gap of about 0.92 eV, with the valence states nearest to the Fermi level having major and minor contributions from V and Cl ions, respectively. This is further substantiated by integrated local density of states (ILDOS) plots near the Fermi energy, as shown in Figure 2(c-d). Spin density plots are shown in Figure 2(e-f), which are similar to the ILDOS plots, barring the fact that the former is localized only at V ions.

To understand the effect of strain on the magnetic (ferroelectric) properties of VOCl_2 monolayer, the energy difference between the FM and remaining three AFM states (the polar displacement in the monolayer) is calculated for each strain percent, as illustrated in Figure 3. Here, the polar displacement is defined as the difference between the fractional coordinates of V ion along the polar axis (a -axis) in the PE and FE state. As shown in Figure 3(a), the energy difference among different magnetic states does not change with lattice parameter a and as a result, AFM3 remains the lowest energy magnetic state. On the other hand, as lattice parameter b is increased, FM becomes the lowest energy magnetic state for 4% and higher strain percent [Figure 3(b)]. Interestingly, an in-plane biaxial tensile strain results a similar magnetic phase transition [Figure 3(c)] around same value of applied strain. This clearly suggests that, ground-state magnetic ordering for the VOCl_2 monolayer depends *ex-*

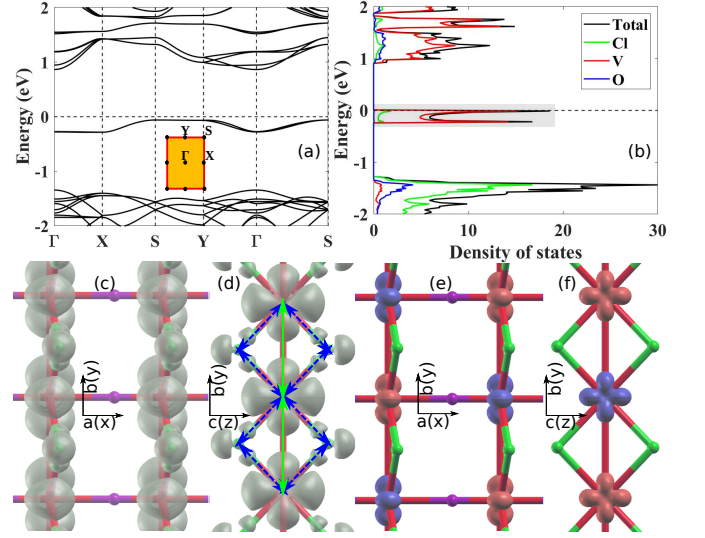


FIG. 2. (a) Electronic band structure and (b) orbital resolved density of states of monolayer VOCl_2 with AFM3 ground state magnetic ordering. High-symmetry points in the first Brillouin zone are also shown in the inset. (c-d) Integrated local density of states (ILDOS), close to the Fermi energy [shaded region in (b)]. In panel (d), solid green lines represent direct exchange interaction between neighboring V-ions and the dashed blue lines represent Cl-mediated super-exchange interaction. (e-f) Spin density localized on V ion, with red and blue color representing opposite spins in AFM3 configuration. ILDOS and spin density plots are prepared using Quantum Espresso⁶¹ and Xcrysden.⁶²

clusively on lattice parameter b , while lattice parameter a has no effect on the magnetic ground state.

The polar displacement, on the other hand, increases monotonically and decreases slightly with increasing lattice parameter a [Figure 3(d)] and b [Figure 3(e)], respectively, irrespective of the magnetic ordering. Since polar displacement is directly related to the spontaneous electric polarization and the primary source for its origin, we find that the spontaneous electric polarization also increases significantly and decreases slightly with tensile strain along the a and b direction, respectively [Figure S2⁵⁹]. Thus, the ferroelectric property can be enhanced either via strain-engineering along the polar axis, or via in-plane biaxial tensile strain as well [Figure 3(f)]. The dynamical stability of the FM-FE VOCl_2 monolayers obtained from in-plane biaxial tensile strain is verified by the phonon spectra, where no imaginary-frequency modes are observed [Figure S3⁵⁹].

So far, our study reveals that, ferroelectric and magnetic properties can be independently controlled via applying strain along the two different in plane crystallographic directions. Therefore, the possibility of engineering both the properties simultaneously via bi-axial strain is explored. As shown in Figure 4(a), spontaneous electric polarization (P_S) values increase monotonically for both AFM3 and FM ordering. The similarity in strain dependence arises possibly because, both AFM3 and FM

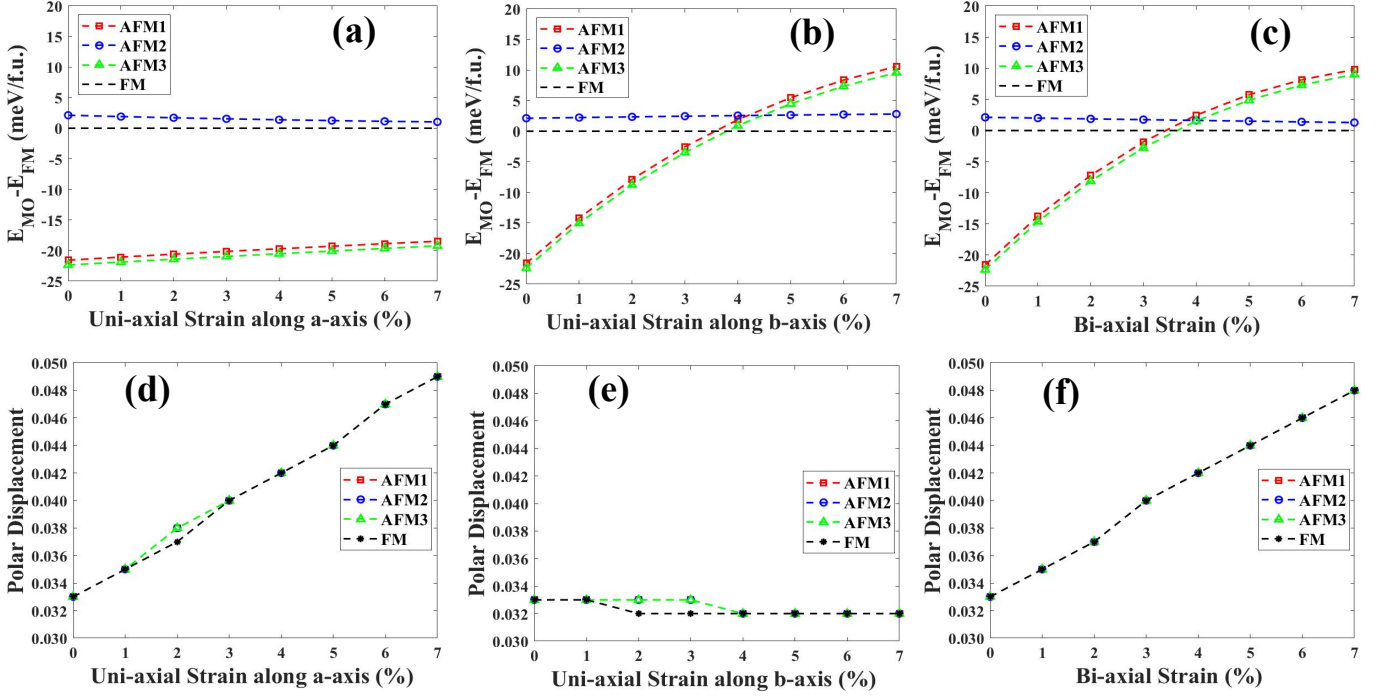


FIG. 3. Variation of energy difference between different magnetic orderings (MO) and FM magnetic ordering [(a), (b), (c)], and dependence of V ion's polar displacement [(d), (e), (f)] in the VOCl_2 monolayer on the uniaxial strain along a -axis [(a), (d)], on the uniaxial strain along b -axis [(b), (e)], and on the in-plane biaxial strain [(c), (f)]. Polar displacement is defined as the difference of the fractional coordinates of V ion along the a -axis in the PE and FE unit cells.

ordering have similar lattice parameters. Nevertheless, P_S values do depend on magnetic ordering, with AFM3 monolayer having marginally higher values of P_S than that of FM for each strain percent, which suggests a weak magnetoelectric coupling, similar to that of type-I multiferroics. Since the polar displacement is almost the same for all the magnetic orderings [Figure 3(f)], thus any difference between the electric polarization values of different magnetic orderings must be arising from electronic contribution, rather than the ionic displacement.

To inspect the stability and robustness of ferroelectric state, the configurational energy barriers for polarization reversal in AFM3-FE and FM-FE VOCl_2 monolayers are determined. Two different polarization switching pathways for the VOCl_2 monolayers are considered. One pathway (Path-1) goes through the intermediate PE phase [Figure 1(e)] and in this case, the activation energy barrier is defined as the depth of the double-well potential (E_G). A monotonic increment in E_G values with bi-axial tensile strain for both AFM3 and FM orderings is observed [Figure 4(b)]. For FM monolayers, these values are slightly lower compared to those of AFM3 monolayers by 5-14 meV/f.u. and the difference increases with bi-axial tensile strain. The second pathway (Path-2) goes through the intermediate antiferroelectric (AFE) phase and in this case, the activation energy barrier is defined as the height of the energy peaks in the FE-AFE-FE transformation (ΔE), as shown in Figure 4(c). This is found to be the pathway with the lowest activation bar-

rier, as reported in literature.³⁶ Similar to E_G , ΔE values also increase with tensile strain [Figure 4(d)]. Initially, AFM3 (magnetic ground state) monolayers have higher ΔE values (by 21 meV/f.u. at zero strain) than those of FM monolayers. However, as the latter becomes the magnetic ground state for a bi-axial tensile strain of 4% and above, ΔE values for the FM monolayer become higher than those of AFM3 monolayers by 2-7 meV/f.u [Figure 4(d)]. Dependence of E_G and ΔE on magnetic ordering is another evidence of weak magnetoelectric coupling present in VOCl_2 monolayers.

Our results so far clearly show that the activation energy barrier for electric polarization switching can be tuned via bi-axial strain and it also depends on magnetic order. This is further investigated by applying uniaxial tensile strain along the in-plane lattice vectors, as shown in Figure S4 (E_G vs. strain) and Figure S5 (ΔE vs. strain)⁵⁹. This confirms that the monotonic increase in both E_G and ΔE values are because of the tensile strain along the polar axis (a -axis). However, the crossover observed in ΔE vs. strain plot of AFM3 and FM phase at 4% bi-axial tensile strain [Figure 4(d)] happens because of the change of b -lattice parameter [Figure S5].⁵⁹

Since E_G values are almost twice the ΔE values for any given magnitude of strain, we conclude that Path-2 [Figure 4(c)] is the one with minimum activation energy, irrespective of the magnitude of strain. Although the AFE phase has energy values close to the FE phase [Figure 4(c)], they are separated by energy barriers rang-

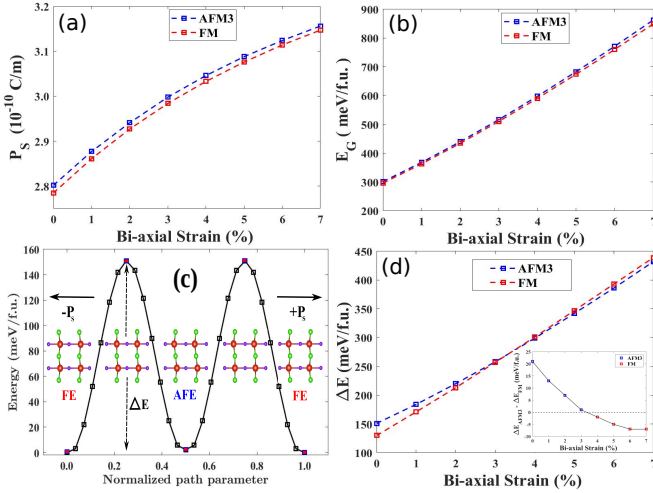


FIG. 4. Influence of the in-plane biaxial strain on the (a) spontaneous electric polarization (P_S) and (b) depth of the double-well potential (E_G). (c) Energy barrier (ΔE) for the polarization switching from $-P_S$ to $+P_S$ via AFE intermediate phase and (d) dependence of ΔE values for AFM3 and FM magnetic state on in-plane biaxial tensile strain. Difference of ΔE in AFM3 and FM magnetic state is shown in the inset of (d).

ing from 151-439 meV/f.u. [Figure 4(d)], which are much larger than the energy of thermal motion at room temperature (25 meV). Thus, these high energy barriers ensures the stability of the FE state. E_G (ranging from 301-863 meV/f.u. and 296-849 meV/f.u. for AFM3 and FM state, respectively) and ΔE (ranging from 151-432 meV/f.u. and 130-439 meV/f.u. for AFM3 and FM state, respectively) values are comparable (or even higher in some cases) to those of typical ferroelectrics such as BaTiO₃ ($E_G = 170$ meV/f.u., $T_c = 393K$), PbTiO₃ ($E_G = 335$ meV/f.u., $T_c = 760K$), and LiNbO₃ ($E_G = 640$ meV/f.u., $T_c = 1483K$),^{63,64} strongly implying the high stability of ferroelectric phase in VOCl₂ monolayers, which further increases with increasing tensile strain along the polar axis.

Having discussed the effect of tensile strain on ferroelectric state of VOCl₂, we now focus on the magnetic state. Increment in the V ion magnetic moment (M_V) with increasing tensile strain is observed in both FE and PE monolayers of AFM3 and FM magnetic state [Figure 5(a)]. FM monolayers are found to have higher M_V , than that of AFM3, in both FE and PE monolayers. Note that, rate of increase of M_V with increasing tensile strain is very small in case of FE monolayers, than compared to PE monolayers, and the latter has slightly higher M_V values as well. This suggests that the magnetoelectric coupling present in VOCl₂ monolayers is rather weak.

To analyze robustness of the magnetic ground state in VOCl₂ monolayers and how it is affected by strain, we calculate the magnetic exchange coupling parameters, as

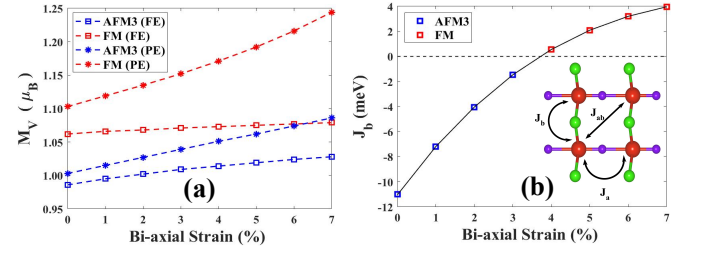


FIG. 5. Influence of the in-plane biaxial strain on (a) V ion's magnetic moment (M_V) and (b) the nearest-neighbor exchange coupling parameter along b-direction (J_b). Black dotted line in (b) represents ground state magnetic order transition from AFM3 to FM.

needed by the following Ising model Hamiltonian,³⁶

$$H = H_0 - \sum_{\langle ij \rangle_a} J_a M_i M_j - \sum_{\langle mn \rangle_b} J_b M_m M_n - \sum_{\langle\langle kl \rangle\rangle} J_{ab} M_k M_l, \quad (1)$$

where H_0 is the non-magnetic Hamiltonian; M_i is the net magnetic moment at site i ; $\langle ij \rangle_a$ ($\langle mn \rangle_b$) corresponds to the nearest-neighbor or NN V atoms along the a -(b)-axis; $\langle\langle kl \rangle\rangle$ stands for the next-nearest-neighbor or NNN V atoms; J_a and J_b are NN magnetic exchange coupling parameters along a - and b -directions, respectively; J_{ab} is the NNN exchange coupling parameter [see Figure 5(b) inset for schematic representation of exchange coupling parameters]. Using the above Hamiltonian, the total energies for four magnetic orderings can be written as:

$$E_{FM} = E_0 - 4M_{FM}^2(J_a + J_b + 2J_{ab}), \quad (2)$$

$$E_{AFM1} = E_0 - 4M_{AFM1}^2(J_a - J_b - 2J_{ab}), \quad (3)$$

$$E_{AFM2} = E_0 - 4M_{AFM2}^2(-J_a + J_b - 2J_{ab}), \quad (4)$$

$$E_{AFM3} = E_0 - 4M_{AFM3}^2(-J_a - J_b + 2J_{ab}). \quad (5)$$

Here, E_0 is the non-magnetic energy, and M_{MO} (where MO = FM, AFM1, AFM2, AFM3) are magnetic moment values for different magnetic orderings. The above four equations are solved using energy and magnetic moment values calculated from our first-principles calculations to obtain the exchange coupling parameters. As can be seen from Table S1⁵⁹, the exchange coupling parameter along b -direction, J_b , is the highest in magnitude among the three coupling parameters for each biaxial and most of the uniaxial strain percent (other than a single exception very close to the magnetic phase transition). Not only J_b values are higher than the rest, but also it changes much more (including a sign reversal) than compared to J_a and J_{ab} with increasing lattice parameter b . This further corroborates the observation that the magnetic ground state depends *exclusively* on the lattice parameter b [Figure 3(a)-(c)].

Having established J_b , which depends on lattice parameter b , as the dominant exchange coupling param-

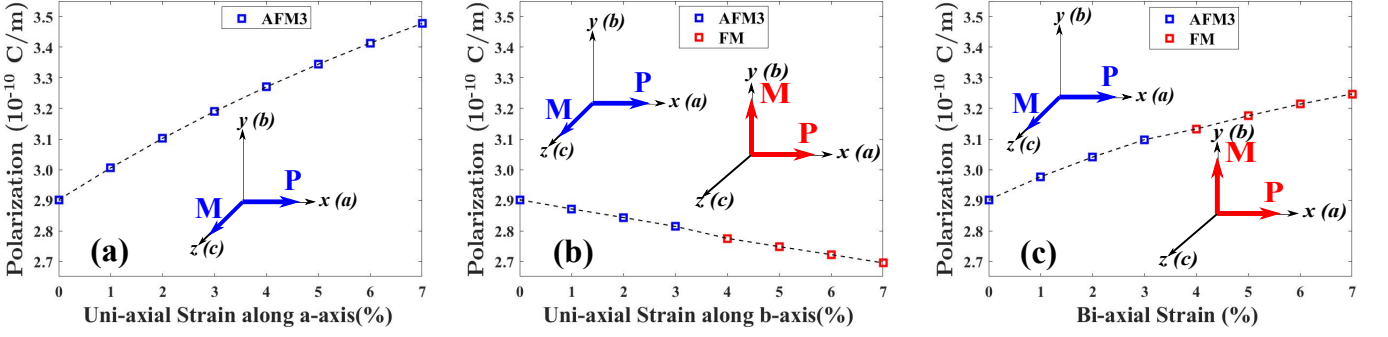


FIG. 6. Variation of spontaneous electric polarization and ground state magnetic ordering in the VOCl_2 monolayer with (a) uniaxial tensile strain along a -axis, (b) uniaxial tensile strain along b -axis, and (c) in-plane biaxial tensile strain. Insets show the direction of magnetic and electric polarization for AFM3 (blue) and FM (red) magnetic ordering. Note the magnetization direction is along $[001]$ (z -axis) and $[010]$ (y -axis) for AFM3 and FM magnetic ordering, respectively. The color of the squares represents the ground state magnetic ordering at that particular strain percent.

eter, we can now qualitatively predict how the magnetic transition temperature changes with strain. As shown in Figure 5(b), value of J_b gradually changes from -11.04 to 3.96 meV with increasing biaxial tensile strain. The crossover from negative to positive values (near 4% strain) signals a change of magnetic ground state from AFM3 to FM. Since a higher magnitude of the J_b value can be related to higher stability of magnetic ordering against thermal fluctuations, we can predict from Figure 5(b) that the Néel temperature (T_N) for AFM3 ground state ordering will decrease, while the Curie temperature (T_C) for FM ground state ordering will increase with biaxial tensile strain. Figure S6 in Supplemental Material⁵⁹ also shows a similar trend for uniaxial strain along the b -axis. We further confirm this by calculating the values of the transition temperatures, using the mean-field approximation,⁶⁵ as reported in Table S2 in Supplemental Material⁵⁹.

For 2D materials, long-range magnetic order stabilization requires lifting of the Mermin-Wagner restriction⁶⁶, which is possible by the presence of magnetic anisotropy^{67,68}. Therefore, taking spin-orbit coupling (SOC) approximation into account, we evaluate the magnetic anisotropy energy (MAE) values for strained VOCl_2 monolayers. We consider magnetization along three in-plane directions: $[100]$, $[010]$, $[110]$, and two out-of-plane directions: $[001]$, $[111]$. From MAE values shown in Table S2 of the Supplemental Material⁵⁹, it is confirmed that the easy axis is along $[001]$ direction and along $[010]$ direction for AFM3 and FM ground state, respectively, both of which are perpendicular to the ferroelectric polarization direction $[100]$. Therefore, AFM3-FE monolayers show out-of-plane magnetization with in-plane ferroelectricity, while FM-FE monolayers show both in-plane magnetization and ferroelectricity in mutually perpendicular directions. Figure 6 illustrates how polarization and ground-state magnetic ordering change in VOCl_2 monolayers with increasing in-plane uniaxial and biaxial tensile strain. The insets in Figure 6 also depict the 90° rotation of the magnetization direction with the change

in the ground-state magnetic ordering around 4% tensile strain. The spontaneous polarization values ranges from 2.9×10^{-10} to 3.3×10^{-10} C/m for in-plane biaxial tensile strain case, which are comparable to the predicted values for 2D ferroelectric monolayer group-IV monochalcogenides (1.51×10^{-10} to 5.06×10^{-10} C/m).¹²

To understand the mechanism behind the ground-state magnetic order transition in VOCl_2 monolayers with tensile strain, we take into account two kinds of exchange interactions among V ions. The first is the direct exchange interaction between the local moments on adjacent V ions [Figure 2(d)], favoring anti-parallel spin alignment.³⁷ In case of VOCl_2 monolayer, neighboring V ions are located closer to each other along the b -axis (3.459 Å), compared to that of a -axis (3.815 Å). As a result, orbitals of neighboring V ions overlap by a relatively larger extent along the b -axis, leading to a strong direct-exchange coupling and a negative J_b value, which is one order of magnitude larger than that of J_a and J_{ab} , both of which have positive sign. However, the change of sign of J_b at 4% tensile strain along the b -direction can not be explained by this model.

The second possibility is a halogen or oxygen mediated superexchange interaction between neighboring V ions. Since V-Cl-V (V-O-V) bonds make an angle of $\sim 90^\circ$ ($\sim 180^\circ$), superexchange interaction is predicted to favor a parallel (antiparallel) spin alignment in neighboring V ions, according to the Goodenough-Kanamori rules.^{69–71} The likelihood of anion mediated superexchange interaction is first checked by looking at the orbital-resolved density of states (DOS) plots [Figure 2(b)], which reveal that the valence states closer to the Fermi level arise mainly from out of the plane V-d orbitals, as well as Cl-p orbitals. Because of the overlap of atomic orbitals with energies close to the Fermi level, it is certainly possible to have a superexchange interaction between nearest neighbor V ions, mediated through Cl ions [Figure 2(d)]. Since O-p levels are located far away from the Fermi energy, O-mediated superexchange mechanism can be ruled out. It is further substantiated by Figure 2(c), which clearly

shows no O-p ILDOS near the Fermi level. From Figure S1⁵⁹, it can be seen that V-Cl bonds are along the b -axis (y -direction), while the V-O bonds are along the a -axis (x -direction). Therefore, the superexchange mechanism, if present, is supposed to be active only along the b -direction.

Our results suggest that the direct-exchange interaction among the neighboring V ions dominate up to 3% tensile strain along the b -axis, promoting AFM3 ordering. As expected, direct-exchange decreases with increasing distance between V ions along the b -direction, which is confirmed by declining magnitude of J_b [see Table S1⁵⁹]. This is further substantiated by the DOS plots at various different tensile strain [Figure S7⁵⁹]. Evidently, the bandwidth decreases with increasing tensile strain, which is a clear signature of decreasing overlap among atomic orbitals. As the distance between neighboring V ions increases further (along b -direction), for tensile strain of 4% and above, the direct-exchange becomes weaker than the halogen mediated superexchange interaction. As mentioned previously, since V-Cl-V bonds make an angle of $\sim 90^\circ$, a ferromagnetic superexchange interaction is possible among neighboring V ions, according to the Goodenough-Kanamori rules;^{69–71} resulting in a positive value for J_b and FM ordering along the b -axis. Unlike J_b , the other two magnetic exchange coupling parameters, J_a and J_{ab} (the latter being always greater than the former, see Table S1⁵⁹) remain almost unchanged for a tensile strain along the b -axis. Since the possibility of oxygen mediated superexchange has already been ruled out, tensile strain along the a -direction has no effect on the magnetic ground state.

Based on the above discussion, evolution of the magnetic ground state as a function of strain can be summarized as following. For a tensile strain ranging from 0-3% (along b -direction, as well as biaxial), negative values of J_b results in anti-parallel spin alignment along the b -axis, while positive values of J_{ab} results in a parallel spin alignment for the diagonally located V ions [Figure 5(b)], yielding the AFM3 ground-state magnetic ordering. For 4% and higher strain percent (along b -direction, as well as biaxial), we obtain positive values for all the exchange coupling parameters, resulting in FM ground-state magnetic ordering. The transition from AFM3 to FM ground state takes place, because the sign of J_b flips [Figure 5(b)] as the Cl-mediated superexchange mechanism becomes dominant at tensile strain of 4% and above.

Violation of the d^0 rule in VOCl_2 monolayer has already been discussed in the literature.³⁷ In order to further check whether d-orbital occupancy has any role on the strain dependence of ferroelectric properties described so far, a TiOCl_2 ferroelectric monolayer is chosen, which has a d^0 configuration for the Ti ion; and polar displacement of the Ti ion (which is proportional to the spontaneous polarization) is calculated [Figure S8⁵⁹]. Similar to the case of VOCl_2 (V d^1), polar displacement in TiOCl_2 (Ti d^0) monolayer also increases with uniaxial tensile strain along the polar axis (a -axis), as well

as biaxial tensile strain but it remains unaffected by the tensile strain along the b -axis. This clearly proves that the enhancement in spontaneous electric polarization for tensile strain along the polar axis is independent of the d-orbital occupancy of the transition metal.

Interestingly, SOC is found to increase the equilibrium lattice parameter of VOCl_2 by nearly 3% [Figure S9⁵⁹]. However, even with SOC, AFM3 is found to be the ground state in equilibrium and it is transformed to a FM state at only $\sim 2\%$ tensile strain [Figure S9⁵⁹], while rest of the physics remain unchanged. A lower value of tensile strain can further increase the chance of realizing such a magnetic phase transition in an experimental set-up. In order to check the robustness of the magnetic ground state, with the inclusion of Hubbard corrections for the localized d-electrons on V ions, DFT+U based calculations are carried out. A qualitatively similar magnetic phase transition from the AFM3 to FM state is observed under uni-axial strain along the b -axis and biaxial strain, for both vdW-DF2 functional [Figure S10⁵⁹] and PBE functional [Figure S11⁵⁹]. Similar to the case of SOC, magnitude of strain required for magnetic phase transition decreases with increasing value of U . Although the bandgap reduces due to the AFM3 to FM transition, the latter is still found to be in an insulating state, with its bandgap increasing further with tensile strain, which is more effective when applied along the polar a -axis, than that of non-polar b -axis [Figure S12⁵⁹].

IV. CONCLUSIONS

In summary, we find VOCl_2 to be a unique multiferroic monolayer, where tensile strain along the polar axis provides (a) high electric polarization, (b) increased ferroelectric stability and (c) enhanced insulating nature; while along the non-polar axis it causes a magnetic phase transition. Moreover, as the ferroelectricity and magnetism can be tuned independently via tensile strain along different in plane crystallographic directions, this material offers a unique opportunity to design 2D type-I multiferroic based nanoelectronic devices, having the flexibility to increase or decrease electric polarization without affecting the monolayer's magnetic properties, and vice-versa. We also find the tensile strain to be beneficial for the purpose of increasing ferroelectric and ferromagnetic Curie temperature of VOCl_2 monolayer. Our work thus reveals the versatility of VOCl_2 , attainable via strain engineering; and this is expected to encourage further theoretical and experimental study of the VOX_2 family of monolayers to realize new multiferroic materials for low-dimensional technologies.

Note added: Recently, we became aware of recent theoretical works on the VOI_2 monolayer,^{72,73} which predict a non-collinear magnetic ground state. However, strength of spin-orbit interactions (being proportional to Z^4 , Z is the atomic number of the halogen atom), which is possibly responsible for the non-collinear magnetic ground

state in VOI_2 , are much smaller in case of VOCl_2 monolayer. Also, a recent study on VOF_2 monolayer,⁷⁴ a new addition to the VOX_2 family, has explored collinear vs. non-collinear magnetic states, and found the former as the actual ground state. Since, Z for Cl ion ($Z=17$) is closer to that of F ion ($Z=9$), than compared to that of I ion ($Z=53$), we expect the VOCl_2 monolayer to have a collinear magnetic ground state, as reported in previous

works as well.^{36,37}

Acknowledgements

We acknowledge funding from SERB (EMR/2017/004970 and CRG/2018/002440). We also thank computer center IIT Kanpur for providing HPC facility.

* amahajan@iitk.ac.in

† bsomnath@iitk.ac.in

- ¹ Hans Schmid, “Multi-ferroic magneto-electrics,” *Ferroelectrics* **162**, 317–338 (1994), <https://doi.org/10.1080/00150199408245120>
- ² Daniel Khomskii, “Classifying multiferroics: Mechanisms and effects,” *Physics* **20**, 1–8 (2009)
- ³ N. A. Spaldin and R. Ramesh, “Advances in magnetoelectric multiferroics,” *Nature Materials* **18**, 203–212 (2019)
- ⁴ Nicola A. Spaldin and Manfred Fiebig, “The renaissance of magnetoelectric multiferroics,” *Science* **309**, 391–392 (2005), <https://science.sciencemag.org/content/309/5733/391.full.pdf>
- ⁵ Martin Gajek, Manuel Bibes, Stéphane Fusil, Karim Bouzehouane, Josep Fontcuberta, Agnès Barthélémy, and Albert Fert, “Tunnel junctions with multiferroic barriers,” *Nature Materials* **6**, 296–302 (2007)
- ⁶ J. F. Scott, “Multiferroic memories,” *Nature Materials* **6**, 256–257 (2007)
- ⁷ J. Wang, J. B. Neaton, H. Zheng, V. Nagarajan, S. B. Ogale, B. Liu, D. Viehland, V. Vaithyanathan, D. G. Schlom, U. V. Waghmare, N. A. Spaldin, K. M. Rabe, M. Wuttig, and R. Ramesh, “Epitaxial bifeo₃ multiferroic thin film heterostructures,” *Science* **299**, 1719–1722 (2003), <https://science.sciencemag.org/content/299/5613/1719.full.pdf>
- ⁸ R. Ramesh and Nicola A. Spaldin, “Multiferroics: progress and prospects in thin films,” *Nature Materials* **6**, 21–29 (2007)
- ⁹ Shuai Dong, Jun-Ming Liu, Sang-Wook Cheong, and Zhifeng Ren, “Multiferroic materials and magnetoelectric physics: symmetry, entanglement, excitation, and topology,” *Advances in Physics* **64**, 519–626 (2015), <https://doi.org/10.1080/00018732.2015.1114338>
- ¹⁰ Jing Ma, Jiamian Hu, Zheng Li, and Ce-Wen Nan, “Recent progress in multiferroic magnetoelectric composites: from bulk to thin films,” *Advanced Materials* **23**, 1062–1087 (2011), <https://onlinelibrary.wiley.com/doi/pdf/10.1002/adma.201003636>
- ¹¹ Wenjun Ding, Jianbao Zhu, Zhe Wang, Yanfei Gao, Di Xiao, Yi Gu, Zhenyu Zhang, and Wenguang Zhu, “Prediction of intrinsic two-dimensional ferroelectrics in in2se3 and other iii2-vi3 van der waals materials,” *Nature Communications* **8**, 14956 (2017)
- ¹² Ruixiang Fei, Wei Kang, and Li Yang, “Ferroelectricity and phase transitions in monolayer group-iv monochalcogenides,” *Phys. Rev. Lett.* **117**, 097601 (2016)
- ¹³ Kai Chang, Junwei Liu, Haicheng Lin, Na Wang, Kun Zhao, Anmin Zhang, Feng Jin, Yong Zhong, Xiaopeng Hu, Wenhui Duan, Qingming Zhang, Liang Fu, Qi-Kun Xue, Xi Chen, and Shuai-Hua Ji, “Discovery of robust in-plane ferroelectricity in atomic-thick snTe ,” *Science* **353**, 274–278 (2016), <https://science.sciencemag.org/content/353/6296/274.full.pdf>
- ¹⁴ Dillon D. Fong, G. Brian Stephenson, Stephen K. Streiffer, Jeffrey A. Eastman, Orlando Auciello, Paul H. Fuoss, and Carol Thompson, “Ferroelectricity in ultrathin perovskite films,” *Science* **304**, 1650–1653 (2004), <https://science.sciencemag.org/content/304/5677/1650.full.pdf>
- ¹⁵ Javier Junquera and Philippe Ghosez, “Critical thickness for ferroelectricity in perovskite ultrathin films,” *Nature* **422**, 506–509 (2003)
- ¹⁶ M. Dawber, K. M. Rabe, and J. F. Scott, “Physics of thin-film ferroelectric oxides,” *Rev. Mod. Phys.* **77**, 1083–1130 (2005)
- ¹⁷ Yandong Ma, Ying Dai, Meng Guo, Chengwang Niu, Yingtao Zhu, and Baibiao Huang, “Evidence of the existence of magnetism in pristine vx_2 monolayers ($x = \text{s, se}$) and their strain-induced tunable magnetic properties,” *ACS Nano* **6**, 1695–1701 (2012), PMID: 22264067, <https://doi.org/10.1021/nn204667z>
- ¹⁸ Hemant Kumar, Nathan C. Frey, Liang Dong, Babak Anasori, Yury Gogotsi, and Vivek B. Shenoy, “Tunable magnetism and transport properties in nitride mxenes ,” *ACS Nano* **11**, 7648–7655 (2017), PMID: 28558192, <https://doi.org/10.1021/acsnano.7b02578>
- ¹⁹ Qisheng Wu, Yehui Zhang, Qionghua Zhou, Jinlan Wang, and Xiao Cheng Zeng, “Transition-metal dihydride monolayers: A new family of two-dimensional ferromagnetic materials with intrinsic room-temperature half-metallicity,” *The Journal of Physical Chemistry Letters* **9**, 4260–4266 (2018), PMID: 30001619, <https://doi.org/10.1021/acs.jpclett.8b01976>
- ²⁰ Chengxi Huang, Junsheng Feng, Fang Wu, Dildar Ahmed, Bing Huang, Hongjun Xiang, Kaiming Deng, and Erjun Kan, “Toward intrinsic room-temperature ferromagnetism in two-dimensional semiconductors,” *Journal of the American Chemical Society* **140**, 11519–11525 (2018), PMID: 30130098, <https://doi.org/10.1021/jacs.8b07879>
- ²¹ Naihua Miao, Bin Xu, Linggang Zhu, Jian Zhou, and Zhimei Sun, “2d intrinsic ferromagnets from van der waals antiferromagnets,” *Journal of the American Chemical Society* **140**, 2417–2420 (2018), PMID: 29400056, <https://doi.org/10.1021/jacs.7b12976>
- ²² Lei Li and Menghao Wu, “Binary compound bilayer and multilayer with vertical polarizations: Two-dimensional ferroelectrics, multiferroics, and nanogenerators,” *ACS Nano* **11**, 6382–6388 (2017), PMID: 28602074, <https://doi.org/10.1021/acsnano.7b02756>
- ²³ Menghao Wu, Shuai Dong, Kailun Yao, Junming Liu, and Xiao Cheng Zeng, “Ferroelectricity in covalently

- functionalized two-dimensional materials: Integration of high-mobility semiconductors and nonvolatile memory,” *Nano Letters* **16**, 7309–7315 (2016), pMID: 27740764, <https://doi.org/10.1021/acs.nanolett.6b04309>
- ²⁴ Anand Chandrasekaran, Avanish Mishra, and Abhishek Kumar Singh, “Ferroelectricity, antiferroelectricity, and ultrathin 2d electron/hole gas in multifunctional monolayer mxene,” *Nano Letters* **17**, 3290–3296 (2017), pMID: 28375621, <https://doi.org/10.1021/acs.nanolett.7b01035>
 - ²⁵ Xiao Tang and Liangzhi Kou, “Two-dimensional ferroics and multiferroics: Platforms for new physics and applications,” *The Journal of Physical Chemistry Letters* **10**, 6634–6649 (2019), pMID: 31600077, <https://doi.org/10.1021/acs.jpclett.9b01969>
 - ²⁶ Qing Yang, Wei Xiong, Lin Zhu, Guoying Gao, and Menghao Wu, “Chemically functionalized phosphorene: Two-dimensional multiferroics with vertical polarization and mobile magnetism,” *Journal of the American Chemical Society* **139**, 11506–11512 (2017), pMID: 28745054, <https://doi.org/10.1021/jacs.7b04422>
 - ²⁷ Zhengyuan Tu, Menghao Wu, and Xiao Cheng Zeng, “Two-dimensional metal-free organic multiferroic material for design of multifunctional integrated circuits,” *The Journal of Physical Chemistry Letters* **8**, 1973–1978 (2017), pMID: 28412811, <https://doi.org/10.1021/acs.jpclett.7b00636>
 - ²⁸ Chengxi Huang, Yongping Du, Haiping Wu, Hongjun Xiang, Kaiming Deng, and Erjun Kan, “Prediction of intrinsic ferromagnetic ferroelectricity in a transition-metal halide monolayer,” *Phys. Rev. Lett.* **120**, 147601 (2018)
 - ²⁹ Yinghe Zhao, Lingfang Lin, Qionghua Zhou, Yunhai Li, Shijun Yuan, Qian Chen, Shuai Dong, and Jinlan Wang, “Surface vacancy-induced switchable electric polarization and enhanced ferromagnetism in monolayer metal trihalides,” *Nano Letters* **18**, 2943–2949 (2018), pMID: 29668292, <https://doi.org/10.1021/acs.nanolett.8b00314>
 - ³⁰ Xiangyang Li, Xingxing Li, and Jinlong Yang, “Two-dimensional multifunctional metal-organic frameworks with simultaneous ferro-/ferrimagnetism and vertical ferroelectricity,” *The Journal of Physical Chemistry Letters* **11**, 4193–4197 (2020), pMID: 32370503, <https://doi.org/10.1021/acs.jpclett.0c01033>
 - ³¹ Xukun Feng, Jian Liu, Xikui Ma, and Mingwen Zhao, “Ferroelectricity and multiferroicity in two-dimensional sc2p2se6 and sccrp2se6 monolayers,” *Phys. Chem. Chem. Phys.* **22**, 7489–7496 (2020)
 - ³² Wei Luo, Ke Xu, and Hongjun Xiang, “Two-dimensional hyperferroelectric metals: A different route to ferromagnetic-ferroelectric multiferroics,” *Phys. Rev. B* **96**, 235415 (2017)
 - ³³ Jingshan Qi, Hua Wang, Xiaofang Chen, and Xiaofeng Qian, “Two-dimensional multiferroic semiconductors with coexisting ferroelectricity and ferromagnetism,” *Applied Physics Letters* **113**, 043102 (2018), <https://doi.org/10.1063/1.5038037>
 - ³⁴ Bao-Wen Li, Minoru Osada, Yasuo Ebina, Shigenori Ueda, and Takayoshi Sasaki, “Coexistence of magnetic order and ferroelectricity at 2d nanosheet interfaces,” *Journal of the American Chemical Society* **138**, 7621–7625 (2016), pMID: 27295544, <https://doi.org/10.1021/jacs.6b02722>
 - ³⁵ Jun-Jie Zhang, Lingfang Lin, Yang Zhang, Menghao Wu, Boris I. Yakobson, and Shuai Dong, “Type-ii multiferroic hf2vc2f2 mxene monolayer with high transition temperature,” *Journal of the American Chemical Society* **140**, 9768–9773 (2018), pMID: 29992814, <https://doi.org/10.1021/jacs.8b06475>
 - ³⁶ Haoqiang Ai, Xiaohan Song, Siyun Qi, Weifeng Li, and Mingwen Zhao, “Intrinsic multiferroicity in two-dimensional voCl2 monolayers,” *Nanoscale* **11**, 1103–1110 (2019)
 - ³⁷ Hengxin Tan, Menglei Li, Haitao Liu, Zhirong Liu, Yuanchang Li, and Wenhui Duan, “Two-dimensional ferromagnetic-ferroelectric multiferroics in violation of the d^0 rule,” *Phys. Rev. B* **99**, 195434 (2019)
 - ³⁸ Nicola A. Hill, “Why are there so few magnetic ferroelectrics?” *The Journal of Physical Chemistry B* **104**, 6694–6709 (2000), <https://doi.org/10.1021/jp000114x>
 - ³⁹ Hua Wang and Xiaofeng Qian, “Two-dimensional multiferroics in monolayer group IV monochalcogenides,” *2D Materials* **4**, 015042 (2017)
 - ⁴⁰ Shiyang Shen, Chang Liu, Yandong Ma, Baibiao Huang, and Ying Dai, “Robust two-dimensional ferroelectricity in single-layer γ -sbp and γ -sbas,” *Nanoscale* **11**, 11864–11871 (2019)
 - ⁴¹ W. Kohn and L. J. Sham, “Self-consistent equations including exchange and correlation effects,” *Phys. Rev.* **140**, A1133–A1138 (1965)
 - ⁴² G. Kresse and J. Furthmüller, “Efficiency of ab-initio total energy calculations for metals and semiconductors using a plane-wave basis set,” *Computational Materials Science* **6**, 15 – 50 (1996)
 - ⁴³ G. Kresse and J. Furthmüller, “Efficient iterative schemes for ab initio total-energy calculations using a plane-wave basis set,” *Phys. Rev. B* **54**, 11169–11186 (1996)
 - ⁴⁴ P. E. Blöchl, “Projector augmented-wave method,” *Phys. Rev. B* **50**, 17953–17979 (1994)
 - ⁴⁵ G. Kresse and D. Joubert, “From ultrasoft pseudopotentials to the projector augmented-wave method,” *Phys. Rev. B* **59**, 1758–1775 (1999)
 - ⁴⁶ John P. Perdew, Kieron Burke, and Matthias Ernzerhof, “Generalized gradient approximation made simple,” *Phys. Rev. Lett.* **77**, 3865–3868 (1996)
 - ⁴⁷ M. Dion, H. Rydberg, E. Schröder, D. C. Langreth, and B. I. Lundqvist, “Van der waals density functional for general geometries,” *Phys. Rev. Lett.* **92**, 246401 (2004)
 - ⁴⁸ Guillermo Román-Pérez and José M. Soler, “Efficient implementation of a van der waals density functional: Application to double-wall carbon nanotubes,” *Phys. Rev. Lett.* **103**, 096102 (2009)
 - ⁴⁹ Kyuho Lee, Éamonn D. Murray, Lingzhu Kong, Bengt I. Lundqvist, and David C. Langreth, “Higher-accuracy van der waals density functional,” *Phys. Rev. B* **82**, 081101 (2010)
 - ⁵⁰ Jiří Klimeš, David R. Bowler, and Angelos Michaelides, “Van der waals density functionals applied to solids,” *Phys. Rev. B* **83**, 195131 (2011)
 - ⁵¹ S. L. Dudarev, G. A. Botton, S. Y. Savrasov, C. J. Humphreys, and A. P. Sutton, “Electron-energy-loss spectra and the structural stability of nickel oxide: An lsd+u study,” *Phys. Rev. B* **57**, 1505–1509 (1998)
 - ⁵² <https://www.ccdc.cam.ac.uk/structures/Home/>, “Link to the inorganic crystal structure database (icsd).”
 - ⁵³ Xavier Gonze and Changyol Lee, “Dynamical matrices, born effective charges, dielectric permittivity tensors, and interatomic force constants from density-functional perturbation theory,” *Phys. Rev. B* **55**, 10355–10368 (1997)

- ⁵⁴ R. D. King-Smith and David Vanderbilt, "Theory of polarization of crystalline solids," *Phys. Rev. B* **47**, 1651–1654 (1993)
- ⁵⁵ Raffaele Resta, "Macroscopic polarization in crystalline dielectrics: the geometric phase approach," *Rev. Mod. Phys.* **66**, 899–915 (1994)
- ⁵⁶ Ankit Izardar and Claude Ederer, "Interplay between chemical order and magnetic properties in Li_0 feni (tetrataenite): A first-principles study," *Phys. Rev. Materials* **4**, 054418 (2020)
- ⁵⁷ A.I. Liechtenstein, M.I. Katsnelson, V.P. Antropov, and V.A. Gubanov, "Local spin density functional approach to the theory of exchange interactions in ferromagnetic metals and alloys," *Journal of Magnetism and Magnetic Materials* **67**, 65 – 74 (1987)
- ⁵⁸ G. H. O. Daalderop, P. J. Kelly, and M. F. H. Schuurmans, "Magnetocrystalline anisotropy and orbital moments in transition-metal compounds," *Phys. Rev. B* **44**, 12054–12057 (1991)
- ⁵⁹ "See supplemental material for: Schematic representation of crystal structure of VOCl_2 monolayer; dependency of polarization on polar displacement; phonon spectra to determine stability of FM-Fe VOCl_2 monolayers; effect of uniaxial tensile strain along in-plane lattice vectors on the ferroelectric switching energy barriers; effect of uniaxial tensile strain along in-plane lattice vectors on the exchange coupling parameter along b -axis; orbital-resolved density of states plots (non-zero tensile strain); polar displacement in TiOCl_2 monolayer with strain; effect of SOC, vdW-df2+u and PBE+u on the energy difference between strained structures; variation of band gap with strain; values of exchange coupling parameters; values of MAE varying with strain; structural parameters for VOCl_2 monolayer under different exchange and correlation functionals."
- ⁶⁰ P. A. Fleury, J. F. Scott, and J. M. Worlock, "Soft phonon modes and the 110°K phase transition in SrTiO_3 ," *Phys. Rev. Lett.* **21**, 16–19 (1968)
- ⁶¹ Paolo Giannozzi, Stefano Baroni, Nicola Bonini, Matteo Calandra, Roberto Car, Carlo Cavazzoni, Davide Ceresoli, Guido L. Chiarotti, Matteo Cococcioni, Ismail A. Dabo, Andrea Dal Corso, Stefano de Gironcoli, Stefano Fabris, Guido Fratesi, Ralph Gebauer, Uwe Gerstmann, Christos Gougousis, Anton Kokalj, Michele Lazzeri, Layla Martin-Samos, Nicola Marzari, Francesco Mauri, Riccardo Mazzarello, Stefano Paolini, Alfredo Pasquarello, Lorenzo Paulatto, Carlo Sbraccia, Sandro Scandolo, Gabriele Sclauzero, and Ari P. Seitsonen, Alexander Smogunov, Paolo Umari, and Renata M. Wentzcovitch, "QUANTUM ESPRESSO: a modular and open-source software project for quantum simulations of materials," *Journal of Physics: Condensed Matter* **21**, 395502 (2009)
- ⁶² Anton Kokalj, "Computer graphics and graphical user interfaces as tools in simulations of matter at the atomic scale," *Computational Materials Science* **28**, 155 – 168 (2003), proceedings of the Symposium on Software Development for Process and Materials Design
- ⁶³ Yubo Zhang, Jianwei Sun, John P. Perdew, and Xifan Wu, "Comparative first-principles studies of prototypical ferroelectric materials by LDA, GGA, and SCAN meta-GGA," *Phys. Rev. B* **96**, 035143 (2017)
- ⁶⁴ Meng Ye and David Vanderbilt, "Ferroelectricity in corundum derivatives," *Phys. Rev. B* **93**, 134303 (2016)
- ⁶⁵ Jozef Strečka and Michal Jascur, "A brief account of the Ising and Ising-like models: Mean-field, effective-field and exact results," *Acta Physica Slovaca* **65**, 235–367 (2015)
- ⁶⁶ N. D. Mermin and H. Wagner, "Absence of ferromagnetism or antiferromagnetism in one- or two-dimensional isotropic Heisenberg models," *Phys. Rev. Lett.* **17**, 1133–1136 (1966)
- ⁶⁷ Yingjie Sun, Zhiwen Zhuo, Xiaojun Wu, and Jinlong Yang, "Room-temperature ferromagnetism in two-dimensional Fe_2Si nanosheet with enhanced spin-polarization ratio," *Nano Letters* **17**, 2771–2777 (2017), PMID: 28441496, <https://doi.org/10.1021/acs.nanolett.6b04884>
- ⁶⁸ Bevin Huang, Genevieve Clark, Efrén Navarro-Moratalla, Dahlia R. Klein, Ran Cheng, Kyle L. Seyler, Ding Zhong, Emma Schmidgall, Michael A. McGuire, David H. Cobden, Wang Yao, Di Xiao, Pablo Jarillo-Herrero, and Xiaodong Xu, "Layer-dependent ferromagnetism in a van der Waals crystal down to the monolayer limit," *Nature* **546**, 270–273 (2017)
- ⁶⁹ John B. Goodenough, "Theory of the role of covalence in the perovskite-type manganites $[\text{La}, m(\text{II})]\text{MnO}_3$," *Phys. Rev.* **100**, 564–573 (1955)
- ⁷⁰ John B. Goodenough, "An interpretation of the magnetic properties of the perovskite-type mixed crystals $\text{La}_{1-x}\text{Sr}_x\text{CoO}_{3-\lambda}$," *Journal of Physics and Chemistry of Solids* **6**, 287 – 297 (1958)
- ⁷¹ Junjiro Kanamori, "Superexchange interaction and symmetry properties of electron orbitals," *Journal of Physics and Chemistry of Solids* **10**, 87 – 98 (1959)
- ⁷² Changsong Xu, Peng Chen, Hengxin Tan, Yurong Yang, Hongjun Xiang, and L. Bellaiche, "Electric-field switching of magnetic topological charge in type-I multiferroics," *Phys. Rev. Lett.* **125**, 037203 (2020)
- ⁷³ Ning Ding, Jun Chen, Shuai Dong, and Alessandro Stroppa, "Ferroelectricity and ferromagnetism in a VOI_2 monolayer: Role of the dzyaloshinskii-moriya interaction," *Phys. Rev. B* **102**, 165129 (2020)
- ⁷⁴ Hai-Peng You, Ning Ding, Jun Chen, and Shuai Dong, "Prediction of two-dimensional ferromagnetic ferroelectric VOF_2 monolayer," *Phys. Chem. Chem. Phys.* **22**, 24109–24115 (2020)